CIRCE2/DEKGEN2: A Software Package for Facilitated Optical Analysis of 3-D Distributed Solar Energy Concentrators[1]

Vicente J. Romero

Fluid and Thermal Sciences Department
Sandia National Laboratories
Albuquerque, New Mexico 87185

SAND--91-1439C

DE92 004215

ABSTRACT

CIRCE2 is a cone-optics computer code for determining the flux distribution and total incident power upon a receiver, given concentrator and receiver geometries, sunshape (angular distribution of incident rays from the sun-disk), and concentrator imperfections such as surface roughness and random deviation in slope. Statistical methods are used to evaluate the directional distribution of reflected rays from any given point on the concentrator, whence the contribution to any point on the target can be obtained. DEKGEN2 is an interactive preprocessor which facilitates specification of geometry, sun models, and error distributions.

The CIRCE2/DEKGEN2 package equips solar energy engineers with a quick, user-friendly design and analysis tool for study/optimization of dish-type distributed receiver systems. The package exhibits convenient features for analysis of "conventional" concentrators, and has the generality required to investigate complex and unconventional designs. Among the more advanced features are the ability to model dish or faceted concentrators and stretched-membrane reflectors, and to analyze 3-D flux distributions on internal or external receivers with 3-D geometries. Facets of rectangular, triangular, or circular projected shape, with profiles of parabolic, spherical, flat, or custom curvature can be handled. Provisions for shading, blocking, and aperture specification are also included.

This paper outlines the features and capabilities of the new package, as well as the theory and numerical models employed in CIRCE2.

1. This work performed at Sandia National Laboratories, supported by the U.S. Department of Energy under contract DE-AC04-76DP00789.

1 INTRODUCTION

Sandia National Labs is actively involved in the design, development, and testing of solar energy collection systems. A significant subset of this effort is directed toward point focus distributed receiver systems. Accordingly, in the mid 1980's, an effort was undertaken to develop a user-friendly capability to model such systems. To predict the distribution of solar flux upon the receivers, HELIOS [1] was chosen as a starting point over other existing optics simulation codes such as CAV [2] and COPS [3] because it contained fewer simplifications and allowed much greater freedom in the receiver and reflector configurations that could be modelled. HELIOS, incorporating much of the mathematical theory developed by Schrenk [4], was developed during the 1970's by Biggs and Vittitoe for modelling the solar central receiver at Sandia. Trough and dish-type systems could also be modelled, but the code's generality made it unnecessarily complex, and cumbersome to use for these applications. In order to facilitate the analysis of point-focus collector systems, Ratzel and Boughton developed CIRCE.001, the "daughter" of HELIOS (as in Greek mythology), and an interactive preprocessor, DEKGEN, to assist in specification of geometry, sun models, and concentrator errors. A plotting capability for 3-D visualization of results was also developed. The analysis code CIRCE.001 (Convolution of Incident Radiation with Concentrator Errors) was easy to run, yet the package had the generality necessary to analyze very diverse concentrator and receiver configurations. This suite of design and analysis tools was reported at the 1987 ASME-JSME Solar Energy Conference [5], and is documented more fully in [6].

Continued work on the CIRCE.001 package over the past several years has lead to a second-generation version: CIRCE2/DEKGEN2 [7]. The most significant additions to the package include: the capability to model 3-D internal or external receivers, improved methodology for simulating facets of custom profile (such as stretched-membrane facets), an improved integration routine for computing total collected power, and control over the process by which concentrator imperfections affect the reflected image. Sever-

al constraints on the types of faceted concentrators that may be correctly modelled have been lifted, provisions for aperturing have been incorporated, and algorithms for blocking and shading have been extended. Additionally, optimization has made the FORTRAN/77 codes even more amenable to execution on personal computers than before. Reductions in CPU-time by factors in excess of 300 have been realized for some practical problems, and storage requirements have been reduced by 95% even though the maximum target grid size for resolution of flux distributions has been increased twenty-fold. The post-processing capability has not been updated because of the many individual preferences in the rapidly changing field of graphic visualization.

This paper surveys the analytical models and numerical procedures employed in CIRCE2. Features and capabilities of the software analysis package are pointed out. Code validation and availability are also addressed.

2 THEORY AND NUMERICAL MODELING

Here the methodology used to simulate the solar image reflected from a real (imperfect) surface is summarized. The contribution of a reflector element to the total solar flux upon the receiver is derived. Additionally, the determination of critical reflector quantities is addressed. Finally, quadrature of the discrete flux distribution (on the target) for determination of total collected power is discussed.

2.1 HELIOS Methodology for Simulating the Solar Image Reflected from a Real Surface

2.1.1 Conceptual Overview

Looking up at the sun, it appears to be a small disk, the brightness and diameter of which are dependent upon atmospheric conditions. Fundamental to solar optics is the treatment of the sun as a disk (not point) energy source. The "sun-disk" usually appears to be brightest at its center, dimmest at the edge. This variation in brightness may be modelled by a probability density function, or "distribution function," as follows. A line drawn from the center of the sun-disk to a point on the earth marks the direction of the "central ray" from the sun to the earth point. A photon incident upon the earth may strike from any of a multitude of directions, depending upon where (on the sun) it originated. Per unit time, more photons are incident from directions associated with the brighter areas of the sun-disk than from those associated with dimmer areas. The directional distribution of incident photons may be described by a probability density function of direction about the central ray. This probability density function is termed the "sunshape" distribution. Thus, as Figure 1 illustrates, the sun effectively irradiates a reflector surface as a cone of rays, and the intensity of radiant energy over the cone angle may vary. Accordingly, statistical cone-optic techniques are employed instead of ray-tracing methods.

For a perfect (ideal) reflector, which has a smooth surface and no absorption, all energy in a given wavelength band incident upon the surface is specularly reflected (angle of incidence = angle of reflection with respect to the surface normal). Thus, the incident and reflected sunshape distributions are identical. Real (imperfect) reflectors, however, have characteristics that cause the reflected sunshape to differ from the incident one. To begin with, some of the energy striking a real surface does not leave because of surface absorption. This is handled by utilizing a specular reflectance parameter, κ, which is assumed to be independent of direction of incidence. Now, in CIRCE2, reflecting surfaces are assumed to

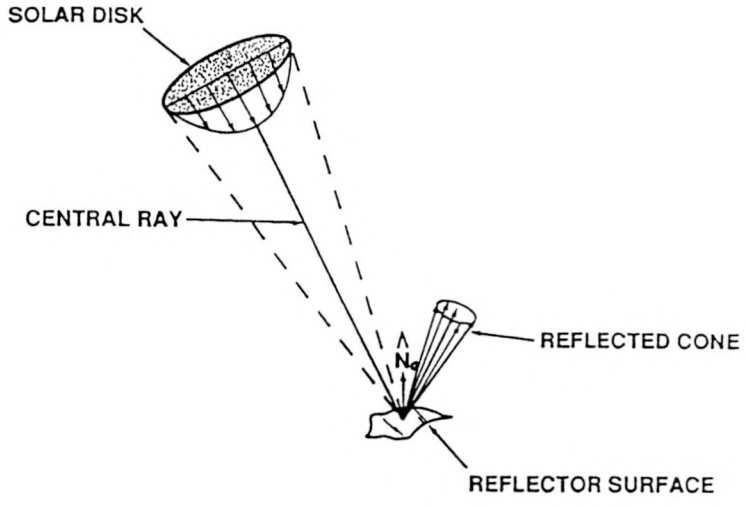

FIGURE 1. Incident and Reflected Solar Images

conform to certain ideal geometries, such as flat, paraboloidal, etc. For these geometries, the "ideal surface normal," $\hat{N}_0$, is unambiguously defined at each point of the surface. The profile of real reflectors, however, will deviate from the ideal shapes, exhibiting some degree of "slope error". Macroscopic imperfections such as surface waviness contribute to the slope error. Additionally, microscopic surface imperfections such as surface striation patterns and surface roughness will cause the actual surface normal, $\hat{N}$, to deviate from the ideal normal. These "concentrator errors" cause the actual surface normal to be nondeterministic; to vary from the ideal surface normal in a manner that is impractical to establish at each point on the reflector. Statistical methods are employed to handle the ambiguity. Each error type can be assigned a probability density function corresponding to the expected standard deviation about $\hat{N}_0$ that $\hat{N}$ will have because of the imperfection. The individual error distributions are combined to produce an overall probability distribution for the direction of $\hat{N}$. Because the distribution represents a multitude of possible surface normal directions, as depicted in Figure 2, it is referred to as the "error-cone."

Now, given a direction of incidence, the ambiguity in the direction of the surface normal results in a distribution of possible reflection directions according to the law of specular reflection. Furthermore, since there is actually a multitude of possible incident directions given by the sunshape, the reflected-ray distribution is a result of the combined effect of both distributions. Figure 2 illustrates this dependence. The incident sunshape is convolved with the error cone to determine the overall probability density function describing the reflected image. This resultant distribution is termed the "effective sunshape."

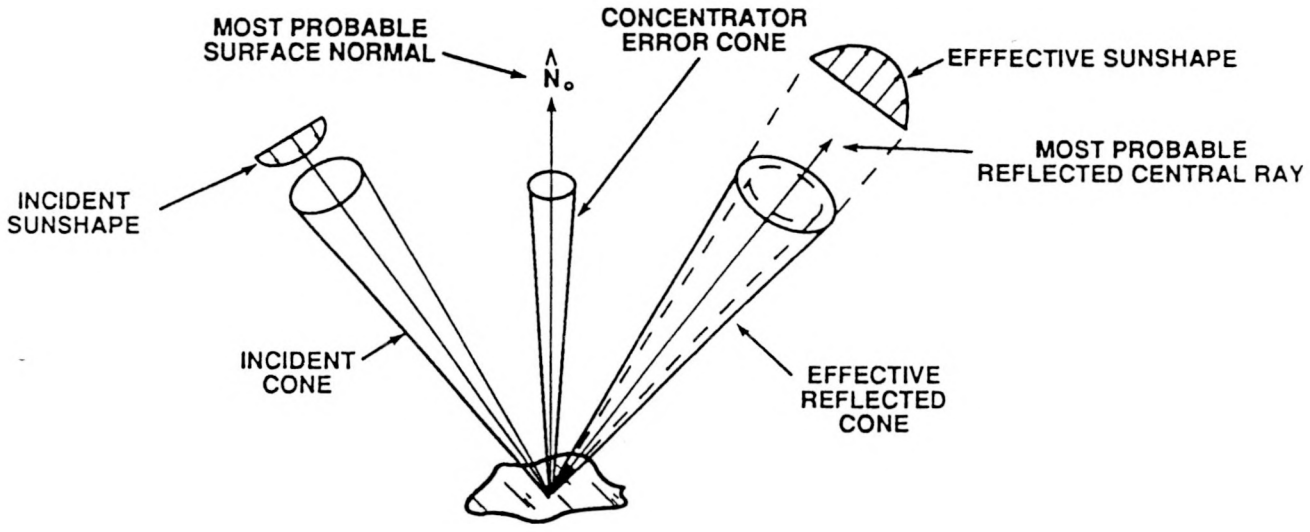

FIGURE 2. Important Distributions in the Statistical Modeling of Solar Reflectors

2.1.2 Calculation of Concentrator Error-Cone

Let the ideal or "most-probable" surface normal $\hat{N}_0$ be a unit normal obtained from a mathematical description of the surface. Concentrator imperfections cause deviations in the direction of the actual surface normal $\hat{N}$ about $\hat{N}_0$. It is assumed that the deviations are randomly distributed and described by 2-D elliptic-normal probability density functions. The form of such a distribution with σ_r and σ_s being the standard deviations in the r- and s- directions, respectively, is:

$$P(r,s) = \frac{1}{2\pi\sigma_r\sigma_s}\exp\left[-\frac{1}{2}\left(\frac{r^2}{\sigma_r^2}+\frac{s^2}{\sigma_s^2}\right)\right] \qquad \text{(EQ 1)}$$

Figure 3 depicts a section of a reflector with $\hat{N}_0$ shown at a point on the surface. Also imposed upon the surface at that point is a rectangular Cartesian coordinate frame called the (ξ,η,ζ) "sun-reflector" coordinate system. The ζ-axis of this system coincides with $\hat{N}_0$. At a unit distance above the surface, parallel to the ξ-η plane, lies the "reflector reference plane." A reference P-Q coordinate system is set up on the plane, whose axes correspond to the ξ-η system translated a unit positive distance along the ζ-axis. Drawn on the plane is a contour of a 2-D elliptic-normal distribution. The r-s coordinate system coincides with the minor and major principal axes of the distribution, respectively. Linear dimensions on the plane are associated with angular deviations from the ideal normal by trigonometry. In practice, the standard deviations in the r- and s- directions are calculated by CIRCE2 upon specification of angular deviations in these directions and the counterclockwise rotation angle θ between the r-s and P-Q axes.

As mentioned previously, the concentrator error-cone is an effective probability density function resulting from the combination of several individual error distributions. Now, if two independent error distributions exist such that each direction of the first distribution is subject to the directional probability described by the second distribution, the resultant effective distribution can be obtained by mathematical convolution of the two distributions. Consider the two elliptic-normal distributions depicted in Figure 4. Only the portions of contours in their respective first quadrants are shown. Their principal axes are separated by the angle Ω. These distributions, $F(r',s')$ and $G(r,s)$, may be convolved to yield the new distribution $h(r,s)$, which is of the form:

$$h(r,s) = c \times \exp\left[-1/2\,(ar^2 + 2krs + bs^2)\right] \qquad \text{(EQ 2)}$$

where a, b, c, and k are constants that depend upon the standard deviations of the distributions and the counter-clockwise (CCW) rotation of the r'-axis from the r-axis. The expression in parentheses is seen to have a quadratic form, allowing it to be expressed as the matrix product <r s>[A]{r,s}. The matrix [A] can be shown [1] to be positive-definite. Thus, the expression in parentheses describes an ellipsoid, for which the cross-term 2krs vanishes under a rotation given by diagonalization of the matrix [A] *cf* [8]. The eigenvectors

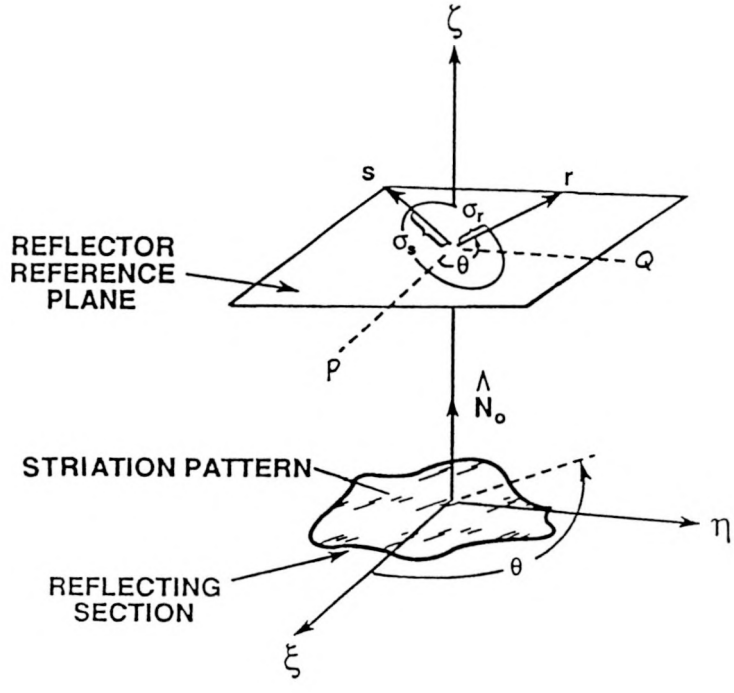

FIGURE 3. Error Distribution on Reflector Reference Plane

FIGURE 4

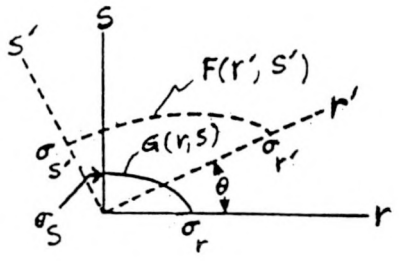

FIGURE 5

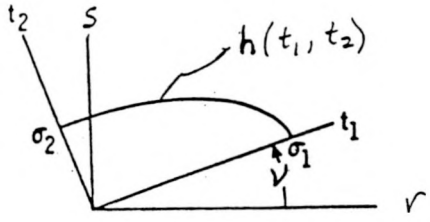

arising from the diagonalization determine the principal axes t1 and t2 of the elliptic-normal distribution h(r,s), and the corresponding eigenvalues give the respective standard deviations σ_1 and σ_2. As shown in Figure 5, the rotation angle ν locates the t1-t2 axes relative to the r-s system. The quantities σ_1, σ_2, and ν may be calculated analytically [1] given the standard deviations of the original distributions F and G, and their separation angle Ω. Thus, convolution of the elliptic-normal distributions F and G may be accomplished analytically, and the only information that must be stored to completely describe the resultant (convolved) distribution h(t1,t2) relative to the r-s coordinate system are the quantities σ_1, σ_2, and ν.

In the above manner, the effect of the next concentrator error is folded-in, convolving its error distribution with the newly acquired distribution h(t1,t2). The process is repeated until all error types are accounted for (up to five are allowed in CIRCE2), yielding the resultant effective error-cone. This distribution may be said to be described by the probability density function C(p,q), having principal axes p and q rotated CCW from the r-s system by the angle λ, with standard deviations σ_p and σ_q. A rotational transformation through the angle δ between the p-q and P-Q coordinate frames ($\delta = \lambda + \theta$) yields C(P,Q), a scalar function of the coordinates P and Q in the reflector reference plane. In the computer code, the error-cone is assumed to be the same at all points on the concentrator surface.

2.1.3 Sunshape Distribution

The intensity, or brightness, of the sun is seen [9-13] to vary from the center to the edge, and to be azimuthally symmetric. The solid angle over which incident solar intensity is non-zero is called the "incident ray cone," as Figure 6 illustrates. A plane is drawn in the figure which is perpendicular to the most-probable reflected central ray, and is at unit distance from the point on the reflector surface. For the moment, let the incident cone of rays experience an undistorted reflection (angle of incidence = angle of reflection) about the most-probable normal $\hat{N}_0$, illuminating the plane as shown. The variation in brightness on the plane can be described by a function S'(ρ), where ρ is measured from the center of the image. Dividing this function by the total reflected power yields a normalized probability density function S(ρ) which, when integrated over the illuminated area, results in a value of unity. This function, when related through trigonometry to the angle γ within the ray cone, describes the directional probability density function Su(γ) that is the sunshape. For the small angles we're concerned with here (on the order of a few milliradians), $\rho = \tan\gamma \approx \gamma$, and the word "sunshape" is used interchangeably in referring to either the distribution in γ or in ρ, the quantities S(ρ) and Su(γ) being essentially the same.

2.1.4 Calculation of Effective Sunshape Distribution

The effective reflected sunshape distribution, ESUN(U,V), is obtained by convolution of the incident sunshape and concentrator error-cone distributions. Before convolution, each distribution is mapped onto the reflected-ray reference plane of Figure 6.

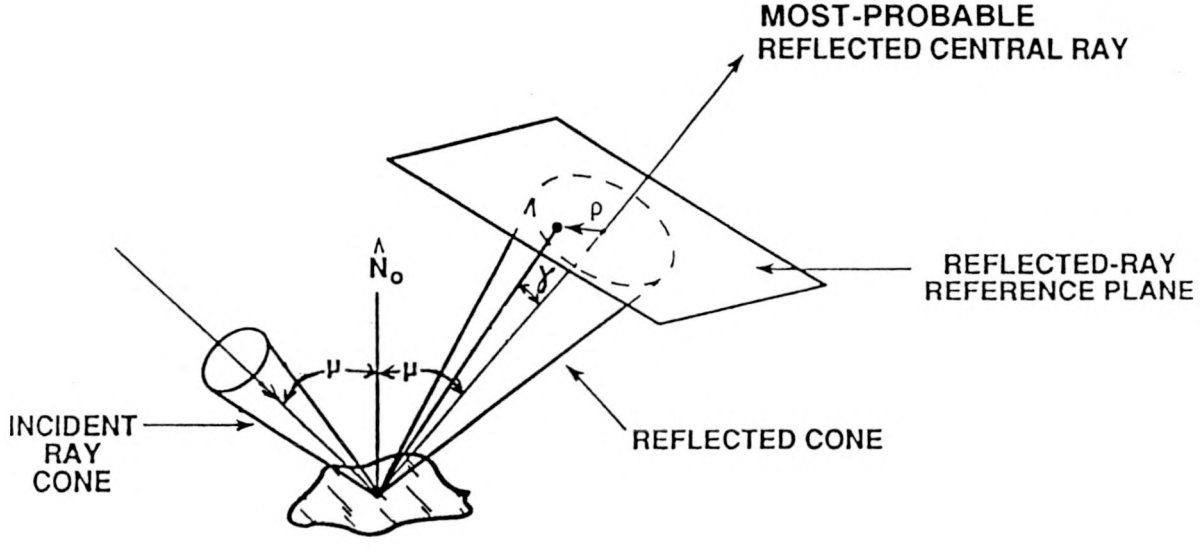

FIGURE 6. Undistorted Solar Image on Reflected-Ray Reference Plane

In general, the concentrator error-cone distribution C(P,Q), being 2-D elliptic-normal in the reflector reference plane (defaulting to 1-D circular-normal if all individual errors are 1-D circular-normal), maps onto the reflected-ray plane as a 2-D elliptic-normal distribution. Figure 7 facilitates explanation of the mapping process. The reference planes associated with the differential reflector element, which were shown separately in Figures 3 and 6, are shown together in Figure 7. The sun-reflector coordinate system is oriented such that the ζ-axis coincides with the most-probable surface normal $\hat{N}_0$ and the η-axis lies in the plane defined by $\hat{N}_0$ and the incident central ray $\vec{A}$. The unit vector $\hat{B}_0$ coincides with the most-probable reflected central ray shown in Figure 6. Imposed upon the reflected-ray reference plane is an orthogonal (U,V) coordinate system with origin at the tip of $\hat{B}_0$. (By definition, both planes are at unit distance from the origin of the sun-reflector coordinate system, though they are not depicted as such in the figure for labeling convenience.) The system is such that the (+) U-axis takes the same direction as the (+) ξ-axis, and the positive direction of the V-axis is as shown. Let the incident ray $\vec{A}$ reflect in the direction $\hat{B}$ according to the actual surface normal $\hat{N}$. The relationship between the (P,Q) coordinates where the extended vector $\hat{N}$ intersects the reflector reference plane, and the (U,V) coordinates where the extended vector $\vec{B}$ intersects the reflected-ray plane, is given (to first-order) by the transformation equations:

$$U = 2P\cos\mu \qquad \text{(EQ 3a)}$$

$$V = 2Q \qquad \text{(EQ 3b)}$$

where the small angle approximation is invoked to obtain equivalent linear dimensions on the planes from angular deviations of the vectors $\hat{N}$ and $\hat{B}$.

It is desired to transform probability in the reflector reference plane to equivalent probability in the reflected-ray plane. Equivalence of differential probability in the two coordinate systems may be written as:

$$C(P,Q)dPdQ = D(U,V)dUdV \qquad \text{(EQ 4)}$$

Noting from (3) that U is a function of P only, and V is a function of Q only, dU = (dU/dP)dP and dV = (dV/dQ)dQ. The relation for invariance , which accounts for the mapping, becomes

$$D(U,V) = C(P,Q)/(4\cos\mu) \qquad \text{(EQ 5)}$$

Equation (5), supplemented with the relations (3a) and (3b), is used to obtain an equivalent concentrator error-cone distribution D(U,V), on the reflected-ray plane, from the distribution C(P,Q) on the reflector reference plane. Thus, these relations, along with the quantities σ_p, σ_q, δ, and μ, fully describe the projected distribution D(U,V). Referred to a set of principal axes u and v, rotated from the U-V system by the angle τ, this elliptic-normal distribution will have standard deviations σ_u and σ_v. The latter three quantities may be obtained analytically from the four former quantities.

Now, there is actually a multitude of possible incident directions about the central ray, as prescribed by the sunshape distribution. Thus, the angle of incidence varies about the value μ, over the cone of incident rays. The transformation relations (3) vary correspondingly. Ideally, the effective probability function describing the angular distribution of rays reflected from the surface would relate, by the method presented above, a differential projected error-cone to a differential solid angle of incident rays. Integrating over the sun-disk, the effective directional distribution of rays coming off of the reflector surface (i.e. effective sunshape) could be obtained. This operation, however, would have to be done numerically, and would introduce large computational expense. The error introduced by treating (3) as constant over the typically very small sun-disk solid angle is extremely small, and as Schrenk [4] speculates, is probably less than the numerical roundoff associated with the computation.

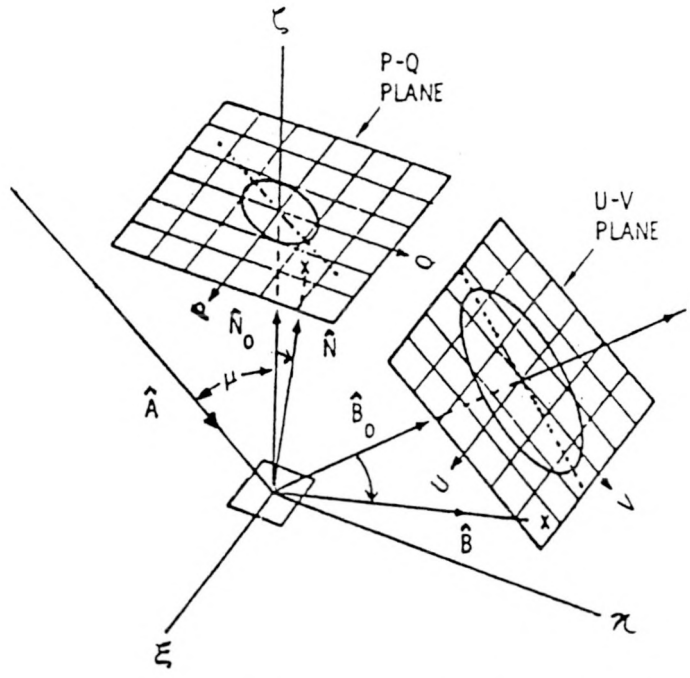

FIGURE 7. Mapping the Concentrator Error Cone from the Reflector (P-Q) Reference Plane to the Reflected-Ray (U-V) Reference Plane.

Once the projected error-cone is obtained, it may be convolved with the projected sunshape (the process is carried out on the reflected-ray plane) to obtain the effective reflected sunshape ESUN(U,V). The incident sunshape is assumed to be a 1-D axisymmetric distribution, though usually not circular-normal because a Gaussian distribution is generally not representative of intensity variation over the solar disk [13]. Strictly, convolution of the projected 2-D elliptic-normal error-cone with the 1-D axisymmetric (not circular-normal) projected sunshape must be done numerically (fast Fourier transforms are used in CIRCE2.) However, several alternatives exist for reducing the cost of this calculation, as cited in section 3.6.

2.2 Determination of Flux at the Target Surface

Knowing the effective sunshape emanating from each point on the reflector, the flux of reflected solar energy upon any point on the target can be obtained. For purposes of numerical computation, the concentrator is usually subdivided into many relatively small reflecting surfaces called "subfacets". Figure 8 shows in schematic a subfacet A_j and target section ΔS_i. Both are flat for convenience in this example. Let the solid angle over which the reflector point "views" the target section intercept the area $\Delta S_{i'}$ on the reflected-ray reference plane. By the definition of solid angle, and recalling that the plane is at unit distance from the reflecting point, the following equality is arrived at:

$$\frac{\Delta S_i \cos\phi}{d^2} = \frac{\Delta S_{i'} \cos\psi}{\sec^2\psi} \qquad \text{(EQ 6)}$$

where d is the distance between points i and j, and $\sec\psi$ is the distance between points i′ and j.

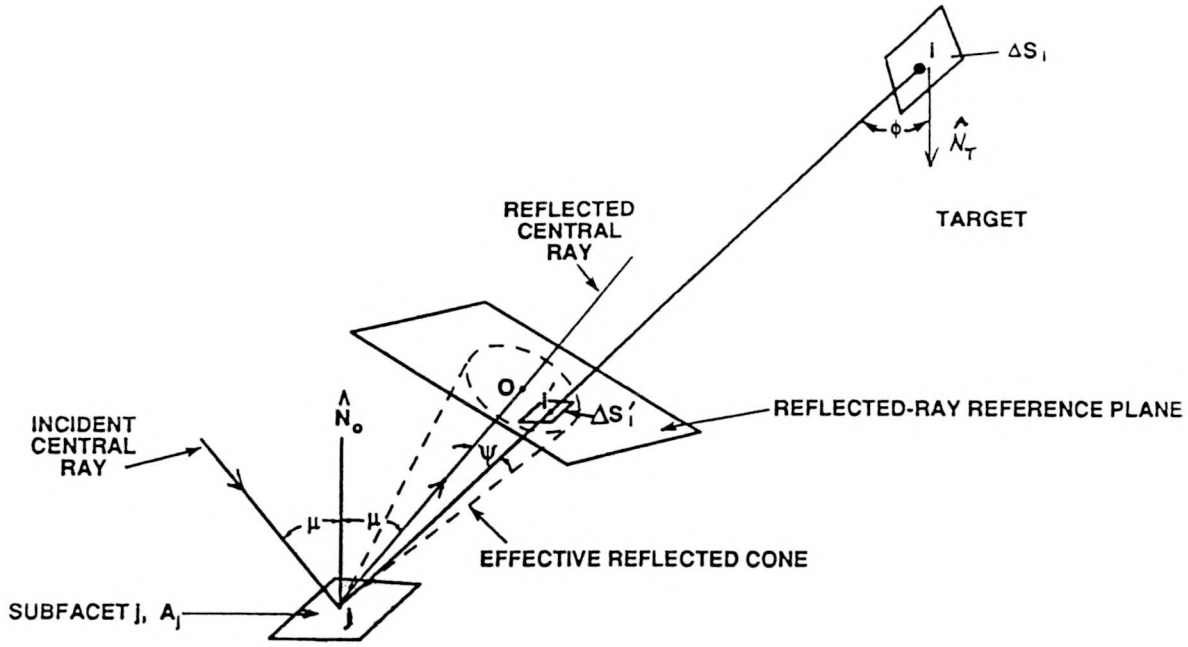

FIGURE 8. Geometric Relationship Between Reflector Element j and Target Point i.

Since they share the same solid angle, ΔS_i and $\Delta S_{i'}$ intercept the same total power. The power intercepted by $\Delta S_{i'}$ is given by the total power coming off the reflector point, κI, multiplied by the differential probability that energy will reflect through $\Delta S_{i'}$. We have:

$$P = \kappa I \times ESUN(U_{i'}, V_{i'})\Delta S_{i'} \qquad \text{(EQ 7)}$$

Using the relation (6) to eliminate $\Delta S_{i'}$ from (7), and dividing both sides by ΔS_i gives the flux at target point i due to reflection from concentrator point j.

$$f_{j-i} = \frac{\kappa I \cos\phi ESUN(U_{i'}, V_{i'})}{d^2 \cos^3\psi} \qquad \text{(EQ 8)}$$

In modelling solar collection systems, several considerations affect the applicability of this equation. On its way from the sun to the concentrator, and then to the receiver, a ray may be stopped in several ways. The receiver itself, or supporting structures, may block rays as they descend upon the concentrator, shading portions of it. Occasionally, some facets may shade themselves and other facets, or block reflected energy. Shading and blocking at the concentrator is accounted by the factor B_j. This factor represents the fraction of the area of subfacet j that is neutralized by shading and blocking. In the vicinity of the receiver, blocking by an aperture is called "aperturing," and is also accounted for. Finally, if the angle ϕ is greater than 90 degrees, the incident rays strike the back side of, or "back-strike," the target, and are not counted.

At this point, an approximation is made to enable numerical solution of the problem we are formulating. All energy reflected from the entire subfacet is assumed to originate from the single point j. Barring aperturing and back-striking, the flux at i due to reflection from subfacet j is given by the product of f_{i-j} and the unneutralized portion of the intercepted reflector area, $(1-B_j)A_j\cos\mu$. Employing equation (8), this becomes:

$$F_{j-i} = \frac{\kappa I \cos\phi \cos\mu (1 - B_j) A_j ESUN(U_{i'}, V_{i'})}{d^2 \cos^3\psi} \qquad \text{(EQ 9)}$$

The total flux at target point i is obtained by summing the contributions of each of the j subfacets on the concentrator.

2.3 Determination of Subfacet Quantities

For each facet of a concentrator, a local *x-y-z* "facet coordinate system" is established. Figure 9 illustrates this coordinate system for a parabolic facet. The mathematical description of the facet's geometry is defined with respect to this coordinate frame. The facet's pojection onto the *x-y* plane forms a circular image, i.e. the facet has a circular "projected shape." In CIRCE2, curved facets are discretized into subfacets by first dividing the projected shape into sections, and then projecting division lines up onto the facet surface. The figure illustrates this correspondence. (Flat facets coincide with their projected shapes, and so division is straightforward.)

For each subfacet, the quantities used in the developments of the previous sections must be established. Continuing with our example, the following approximations are made in the code. Referring to Figure 9, the centroid of the shaded element on the x-y plane is determined. Projecting this point up onto the facet defines the location of the source-point j for the subfacet. The most probable normal, $\hat{N}_o$, is taken to be perpendicular to the facet surface there, rising off of the concentrating (concave) side. The area A_j of the subfacet is approximated by dividing the area of the shaded element in the *x-y* plane, projected area A_j^P, by the dot product of $\hat{N}_o$ and $\hat{z}_k$, where $\hat{z}_k$ is a unit vector along the (+) *z*-axis of the k^{th} facet's local coordinate system.

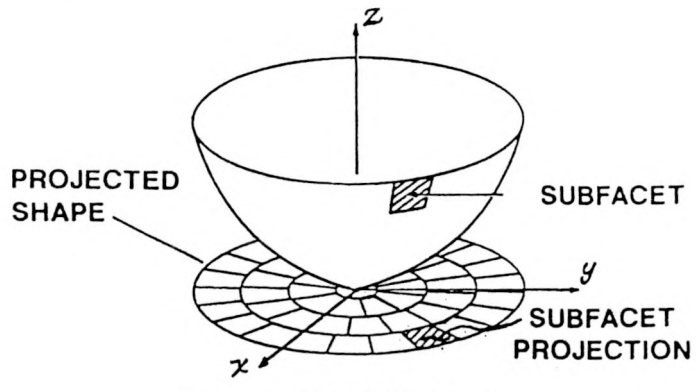

FIGURE 9. Parabolic Facet

2.4 Determination of Total Power Intercepted by Target

To determine total collected power, the normally incident flux at a regular pattern of grid points on the target surface is evaluated, from which a numerical integration yields total power. Here, "regular" means: at intervals on the target surface described by equi-incremental stations of the curvilinear coordinates which describe the surface. Figure 10 may be used for clarification. Shown is a spherical target section, which is completely described by variations of the coordinates Θ and φ on the surface defined by the equation ρ=constant. The total angular extents $\Delta\Theta$ and $\Delta\varphi$ are divided into equal increments $\delta\Theta$ and $\delta\varphi$, such that $\Delta\Theta = n\delta\Theta$ and $\Delta\varphi = m\delta\varphi$. An orthogonal net of lines is formed on the surface with $\delta\Theta$ and $\delta\varphi$ spacing. The grid of points located by the intersections of the mesh lines represents a "regular" discretization of this two-coordinate surface.

Integration of the flux distribution on the receiver is accomplished by numerically integrating over subsections of 3x3 grid points and summing the results over all subsections. The quadrature is performed over a flat, rectangular domain in the surface coordinates. For example, in the spherical case, the surface integral becomes:

$$\iint_R F(\Theta,\varphi)\,\rho^2 \sin\varphi\, d\Theta\, d\varphi = \iint_R F^*(\Theta,\varphi)\, d\Theta\, d\varphi \qquad \text{(EQ 10)}$$

where $F(\Theta,\varphi)$ is the flux distribution on the target. Orthogonal coordinates Θ and φ can be visualized to preside over a flat domain upon which the scalar function F^* is defined. The grid of points becomes rectangular and equi-spaced in this domain, and the value of F^* is known at each of the points. Numerical quadrature is simply a matter of choosing a weighting scheme for the values at the points. The weighting technique that is used in CIRCE2 has been found [7] to be particularly accurate for integrating the circular-periodic flux distributions of axisymmetric targets, while retaining the same accuracy as the methods employed in HELIOS for flat, rectangular targets. Moreover, it is just as fast as the HELIOS methods. It amounts to a trapezoidal rule in the azimuthal coordinate, where flux variations are relatively small, combined with a Simpson's rule weighting in the orthogonal direction, where flux variations are usually higher. For flat rectangular and circular targets, the method yields results that agree extremely well with those of the sophisticated (and computationally expensive) integrator used in CIRCE.001, which couples an 8-point adaptive Legendre-Gauss fit in one direction with a 7-point Newton-Cotes adaptive scheme in the other.

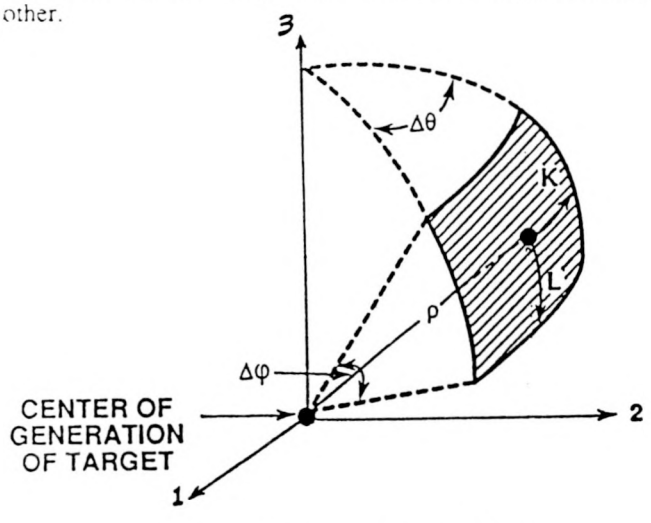

FIGURE 10. Spherical Target Section

3 PACKAGE FEATURES AND CAPABILITIES

3.1 Interactive Preprocessor

DEKGEN2 is an interactive preprocessor module that guides the user through the process of building and discretizing the concentrator and receiver, defining the concentrator error distributions, and specifying a sun model. The code has the capability to read data files, such as tabular sunshapes and facet data, that are used repeatedly or are most efficiently generated by separate computer program. Where possible, DEKGEN2 checks to ensure that data input is consistent with previous information and/or within the acceptable ranges of the parameters. The code then creates the data deck necessary to run the analysis module CIRCE2.

3.2 Concentrator Modeling

Concentrator geometry is defined relative to an absolute X-Y-Z "collector reference frame," as shown in Figure 11. The sun position is specified by defining a vector in this reference frame that locates the sun. Effects of instantaneous tracking errors may be investigated by aligning the concentrator axis with the global Z-axis, and then specifying an off-axis "sun vector."

Up to 250 facets are located on the concentrator by specifying the (X,Y,Z) coordinates of their vertexes. (The vertex of each facet marks the origin of its local facet coordinate system.) Facets can be "aimed" in either of two ways. The user can specify the direction cosines of the facet-system *z*-axis. Alternatively, the user may define up to 50 "aim points" as shown in the figure, each being assigned an integer identifier and (X,Y,Z) coordinates. Each facet may then be associated with any one of the aim points through a correspondence list. The facets are internally aimed (temporarily assuming the sun to be overhead along the collector Z-axis) such that the reflected central ray from the vertex of each facet goes through its associated aim point. Facets of rectangular and triangular projected shape may also be individually rotated about their *z*-axes to obtain the desired orientation.

Concentrator modelling must include the effects of shading and blocking. The receiver itself, or supporting structures, may block rays as they descend upon the concentrator, shading portions of it. Occasionally, some facets may shade themselves and other facets, or block reflected energy. For concave facets, self-blocking

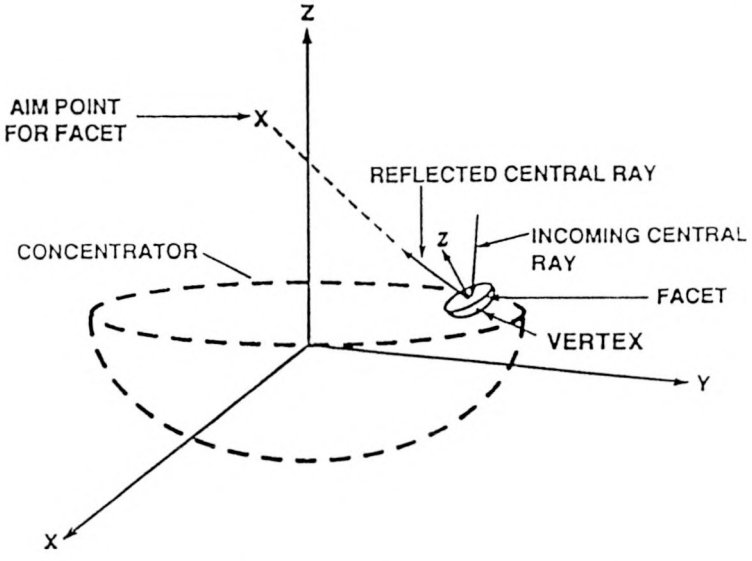

FIGURE 11. Elements of Concentrator Modeling

and self-shading are checked and accounted for. Shading of the concentrator by the target/support structure can be handled in a number of ways. The user may input, individually for each facet, a factor B_j corresponding to the fraction of surface that is shaded, which can also include the fraction of the surface whose reflected rays are being blocked. This fraction is assumed to apply to all subfacets of the facet. Alternatively, the user may orient a circular or rectangular planar shape above the concentrator such that it emulates the receiver. The shadow it casts on the concentrator is calculated internally, depending upon the sun position, and subfacets are assigned a shading factor B_j according to the portion of the surface intercepted by the shadow.

3.3 Facet/Subfacet Modelling

Facet geometry is described by "contour" or "profile," and "projected shape." Facets of circular, rectangular, or triangular projected shape may be specified. The package affords control over the level of discretization of the projected shapes, thus the number of elements into which the facets are divided (see Section 2.3.)

Regarding contour, a facet has a characteristic shape that is produced by rotation of a curve about the facet coordinate system z-axis. The curve is assumed to originate at the origin of the x-y-z system, to be single-valued (does not pass over itself), and to be monotonically increasing (inflection points permissible). CIRCE2 handles the standard parabolic, spherical, and flat profiles, as well as more customized shapes, such as those characteristic of stretched-membrane reflectors. The profile curve for custom shapes can be described by one of three methods: i) polynomial (up to 10th order) where the order and coefficients must be supplied; ii) linear interpolation or cubic spline fit of a table of radius vs. z data (up to 99 data points possible); iii) same as option (ii), but the user inputs most-probable normals. Each of these options has attributes over the others for certain data sets, as explained at length in [7].

3.4 Target/Receiver Modelling

CIRCE2 and DEKGEN2 support the generation and analysis of flat rectangular or circular targets, or 3-D internal or external receivers of cylindrical, spherical, or conical (upright or inverted) shape. Targets are not limited to "complete" shapes, i.e., just the frustrum of a cone may be analyzed, or a small angular section of the frustrum, as opposed to the full axisymmetric region. Up to a 51x51 grid of points may be imposed upon the targets for resolution of the flux distribution. Moreover, "hybrid" receivers built from axisymmetric cylindrical, spherical, conical, and flat-circular components may be constructed, with up to a 51x51 grid assignable to each component. For axisymmetric targets, receiver aperturing is automatically accounted for, and can be separately specified for other targets. Thus, the package is particularly well suited to evaluation of axisymmetric cavity-type receivers.

3.5 Sunshape Modelling

In measuring the intensity variation over the sun-disk, power is usually given as a function of the angle from the central ray. This distribution is called the sunshape. In analysis, it is convenient to separate the total insolation I from the "shape" of the distribution by normalizing the input distribution. After normalization, this distribution (also called the sunshape) constitutes the probability density function represented as $S(\rho)$ in Section 2.1.3. CIRCE2 requires input of total insolation I as well as some distribution (which is internally normalized if necessary) to indicate shape. Provisions exist for inputing the distribution by i) tabular data; ii) specification of standard deviation and ultimate width for a Gaussian distribution; or iii) specifying width and choice of one of six "limb-darkening" options for a uniform "top-hat" distribution.

3.6 Control over Calculation of Effective Sunshape

In general, the effective reflected sunshape ESUN(U,V) *(cf* Section 2.1.4) varies from point-to-point on the concentrator because, though the error-cone C(P,Q) and incident sunshape $S(\rho)$ are assumed to be invariant, the incidence angle μ may vary. Thus, the relative positioning of the reflector- and reflected-ray reference planes of Figure 7 changes from point-to-point on the concentrator. Accordingly, the projected distribution D(U,V) on the reflected-ray plane varies, and along with it, the product distribution ESUN.

Calculation of the effective sunshape may be the dominant computational operation in a CIRCE2 simulation if it is done at many points on the concentrator. However, undercalculation leads to greater error. It is advantageous to be able to tailor this computation to the resources and goals of the analysis. In many cases, it is appropriate, or necessary, to approximate ESUN as being constant over a facet or group of facets. In this case, CIRCE2 sets up, at each subfacet in the group, a reflected-ray reference plane with appropriate U-V coordinate axes. An invariant effective sunshape over that group of subfacets, ESUN'(U,V), is used in the calcalculations of section 2.2. CIRCE2 may be directed to calculate a new effective sunshape at: i) every subfacet; ii) the center of each facet (effective sunshape invariant over the facet) ; iii) the center of only one facet (effective sunshape invariant over entire concentrator).

The cost of the calculation of the effective sunshape may also be moderated, at the expense of some accuracy, by using approximate analytic methods instead of a numerical computation. One option is to convert the 1-D sunshape (usually not prescribed as a circular-normal distribution) into a 1-D circular-normal distribution having the same *rms* width as the prescribed sunshape, and then to perform the convolution with the 2-D elliptic-normal projected error cone analytically. Another is to approximate the projected error-cone by an *rms*-equivalent 1-D circular-normal distribution, simplifying convolution with the 1-D sunshape, whether numerically or analytically performed.

4 CODE OPTIMIZATION AND VALIDATION

While capabilities of CIRCE2/DEKGEN2 have been significantly extended relative to CIRCE.001/DEKGEN [5,6], computational and storage requirements have been reduced dramatically. CIRCE2 requires only 5% of the storage that CIRCE.001 does. Additionally, optimization of the code has resulted in large computational savings - reductions in CPU time of over three orders of magnitude have been realized on a VAX/8800 for some practical problems. These attributes make the current code even more amenable to execution on personal computers.

Where they have common capabilities, CIRCE2 has been checked extensively against its predecessor, CIRCE.001, which has seen substantial use at Sandia National Labs and elsewhere. CIRCE.001, being a direct descendent of HELIOS [1], was checked extensively against that code (see [5,6] for some of the benchmark cases run, and timing studies performed, on CRAY, VAX and PC machines.) The CIRCE2/DEKGEN2 package has been used, primarily by Sandia researchers, in recent analyses published in the solar energy literature [14-20]. (Several of these are to be presented at this conference.) This body of work has provided an indirect,

semi-quantitative validation of CIRCE2. More directly, flux distributions on flat targets recorded by the Sandia Video Flux-Mapping System, and calibrated by flux gauges in the target, have been visually compared against images predicted by CIRCE2. However, the comparisons have been subjective, relying on visual judgement. As reported in [16], software and a methodology are now available to quantitatively compare real image measurements against theoretical predictions. It would be necessary to apply these tools with the specific goal of benchmarking CIRCE2 before a conclusive, fully quantitative assertion could be made regarding the code's validity.

5 CONCLUSIONS, AVAILIBILITY

Considerable practical use of the CIRCE2/DEKGEN2 software package has resulted in a robust and user-friendly product. More work must be done to verify the analysis code, but the tools apparently now exist to do this quantitatively.

Our objective is to release the package for general use in early 1992. The codes are written in standard FORTRAN/77, and run interchangeably on our VAX/VMS and PC/DOS systems.

ACKNOWLEDGEMENTS

I would like thank A. C. Ratzel, from whom I inherited the codes, for his help and advice. Thanks also to R. B. Diver who drove the effort and tested the software, and to T. R. Mancini, whose applications necessitated many of the advanced features the package now contains. Commendations go to F. Biggs and C. N. Vittitoe for their diligent documentation of the mathematical models and numerical procedures used in the HELIOS code. Finally, I would like to cite the work that Roy Hogan did in devising an improved target flux integration scheme.

REFERENCES

[1] Biggs, F., and Vittitoe, C.N., "The HELIOS Model for the Optical Behavior of Reflecting Solar Concentrators," Sandia National Laboratories report SAND76-0347, 1976 ---- 1979 printing available through the National Technical Information Service, U.S. Department of Commerce.

[2] Wan, C.C., "CAV Code for the Determination of Incident Flux Distribution in an Axisymmetrical Cavity from a Parabolidal Reflector," Ford Aerospace & Communications Corp. Technical Report SCSE-016, July, 1980.

[3] "Concentrator Optical Performance Software (COPS)," user's manual, Honeywell Report DOE/CS/35348-T1 (Vol.2), January, 1980.

[4] Schrenk, G.L., and Gritton, D.G., "Analysis of Solar Reflectors - Mathematical Theory and Methodology for Simulation of Real Reflectors," Allison Division of General Motors Corp., report GMC-AO-EDR3693, December, 1963.

[5] Ratzel, A.C., Boughton, B.D., Mancini, T.R., and Diver, R.B., "CIRCE: A Computer Code for the Analysis of Point-Focus Solar Concentrators," *Proceedings of the 1987 ASME-JSME Solar Energy Conference*, Honolulu, Hawaii, March 22-27, 1987.

[6] Ratzel, A.C., and Boughton, B.D., "CIRCE.001: A Computer Code for Analysis of Point-Focus Concentrators with Flat Targets," Sandia National Laboratories Report SAND86-1866, printed February, 1987.

[7] Romero, V.J., "CIRCE2/DEKGEN2: A Software Package for Facilitated Optical Analysis of 3-D Distributed Solar Energy Concentrators -- Theory and User Manual." Sandia National Laboratories report SAND91-2238, in review.

[8] Strang, G., *Linear Algebra and its Applications*, 2nd ed., Chapter 6, Harcourt Brace Jovanovich, Inc., 1980.

[9] Grether, D., and Hunt, A., "Description of the LBL Reduced Data Base and Standard Profiles," Lawrence Berkely Laboratory, August 9, 1977.

[10] Kuiper, G.P., editor, *The Sun, The Solar System*, University of Chicago Press, Chicago, IL, 1953.

[11] Pettit, R.B., Vittitoe, C.N., and Biggs, F., "Simplified Calculational Procedure for Determining the Amount of Intercepted Sunlight on an Imaging Solar Concentrator," *ASME Journal of Solar Energy Engineering*, Vol. 105, February, 1983.

[12] Rosen, M.A., "The angular Distribution of Diffuse Sky Radiance: An Assessment of the Effects of Haze," *ASME Journal of Solar Energy Engineering*, vol. 113, August, 1991.

[13] Vittitoe, C.N., and Biggs, F., "Six-Gaussian Representation of the Angular-Brightness Distribution for Solar Radiation," *Solar Energy*, vol. 27, no. 6, Pergamon Press, 1981.

[14] Adkins, D.R., and Rawlinson, K.S., "Critical Issues in the Develpment of Hybrid Solar/Gas Receivers for Dish/Sterling Systems," *Proceedings of the 1992 ASME-JSES-KSES International Solar Energy Conference*, Maui, Hawaii, April 4-8, 1992.

[15] Diver, R.B., "Reflux Solar Receiver Design Considerations," *Proceedings of the 1992 ASME-JSES-KSES International Solar Energy Conference*, Maui, Hawaii, April 4-8, 1992.

[16] Grossman, J.W., Houser, R.M., and Erdman, W.W., "Prototype Dish Testing and Analysis at Sandia National Laboratories," *Proceedings of the 1992 ASME-JSES-KSES International Solar Energy Conference*, Maui, 1992.

[17] Hogan, R.E., "AEETES - A Solar Reflux Receiver Thermal Performance Numerical Model," *Proceedings of the 1992 ASME-JSES-KSES International Solar Energy Conference*, Maui, 1992.

[18] Hogan, R.E., "Numerical Modeling of Dish-Sterling Reflux Solar Receivers," *Proceedings of the 1991 ASME Solar Engineering Conference*, Reno, Nevada, March 17-22, 1991.

[19] Mancini, T.R., "Analysis and Design of Two Stretched-Membrane Parabolic Dish Concentrators," *ASME Journal of Solar Energy Engineering*, vol. 113, August, 1991.

[20] Moreno, J.B., Andraka, C.E., Diver, R.B., Moss, T.A., Hoffman, E.L., and Stone, C.M., "Reflux Pool Boiler as a Heat-Transport Device for Stirling Engines: Postmortem Analysis and Next-Generation Design," *Proceedings of the 26th Intersociety Energy Conversion Engineering Conference*, Boston, MA, August4-9, 1991.